Calhoun

Institutional Archive of the Naval Postgraduate School

Calhoun: The NPS Institutional Archive

Faculty and Researcher Publications | Faculty and Researcher Publications Collection

2003-12

On the Development of GNC Algorithm for a High-Glide Payload Delivery System

Kaminer, I.

Kaminer, I., and Yakimenko, O., "On the Development of GNC Algorithm for a High-Glide Payload Delivery System," Proceedings of the 42nd IEEE Conference on Decision and Control, Maui, HI, December 8-12, 2003.

On the Development of GNC Algorithm for a High-Glide Payload Delivery System

Isaac I. Kaminer and **Oleg A. Yakimenko**
Department of Mechanical Engineering, Naval Postgraduate School, Monterey, CA 93943
{kaminer,oaykime}@nps.navy.mil

Abstract - The paper considers the development and simulation testing of the control algorithms for an autonomous high-glide aerial delivery system, which consists of 650*sq.ft* rectangular double-skin parafoil and 500*lb* payload. The paper starts with the optimal control analysis and applies it further to the real-time trajectory generation. Resulting guidance and control system includes tracking this reference trajectory using a nonlinear tracking controller. The paper presents the description of the algorithm along with simulation results.

I. INTRODUCTION

Autonomous parafoil capability implies delivering the system to a desired landing point from an arbitrary release point using onboard computer, sensors and actuators. This requires development of a guidance, navigation and control (GNC) system. The navigation subsystem manages data acquisition, processes sensor data and provides guidance and control subsystems with information about parafoil states. Using this information along with other available system data (such as local wind profiles), the guidance subsystem plans the mission and generates feasible (physically realizable and mission compatible) trajectory that takes the parafoil from the initial position to the desired landing point. Finally, it is the responsibility of the control system to track this trajectory using the information provided by the navigation subsystem and onboard actuators.

In the past decade, several GNC concepts for gliding parachute applications have been developed and published (see [1] and references therein). Most of them were tested in a simulation environment, some in flight test.

Present paper addresses the problem of GNC development for a parafoil system as follows. First, a feasible trajectory is generated in real-time that takes the parafoil from initial release point to touch down at a desired impact point. It is assumed that only the direction of the wind at the landing zone (LZ) is known. The trajectory consists of an initial glide, spiral descent and of final glide and flare. The final glide and flare are directed into the wind at LZ. This structure is motivated by optimal control analysis carried out on a simplified model. The resulting trajectory is tracked using a nonlinear algorithm with guaranteed local stability and performance properties [2]. The control algorithm converts trajectory-tracking errors directly into control actuator commands. Therefore, only GPS position and velocity are needed to implement it.

As expected the basic trajectory structure is similar to the ones reported in the literature. However, as shown in Section II, a single smooth inertial trajectory is generated using simple optimization and is tracked throughout the drop by the same control algorithm. This eliminates the need for multiple modes, extensive switching logic and wind information throughout the drop. The latter is made possible by the nonlinear control algorithm that tracks the inertial trajectory directly and treats wind as a disturbance.

The specific delivery system considered in this paper is called Pegasus. It consists of 650*sq.ft* span rectangular double-skin parafoil and 500*lb* payload and was originally manufactured by the FXC Corp. It can be controlled by symmetric and differential flap deflections that occupy outer four (out of eight on each side) cells of the parafoil.

A complete six-degree-of-freedom (6DoF) model of Pegasus was developed and tuned using flight test data provided by the US Army Yuma Proving Ground, AZ (YPG) [3]. This model matches flight test data and is characterized by the following integral parameters: the average descent rate is 3.7-3.9*m/s*, glide ratio is about 3.0, the turn rate of ~6°/s corresponds to the full deflection of one flap. An interesting feature from the control standpoint is that the system exhibits almost no flare capability (flaps deflection results in almost no change in the descent rate). Therefore, it is very important to land it into the wind.

This paper is organized as follows. Section II introduces optimal control strategy for a simplified parafoil model using Pontrjagin's principle of optimality. Section III discusses real-time trajectory generation for the control algorithm. Section IV discusses the development of the tracking control algorithm. Section V introduces simulation results of the complete guidance and control system. Finally, Section VI contains the main conclusions.

II. OPTIMAL CONTROL SYNTHESIS

Consider the following kinematic model of a parafoil in the horizontal plane. Suppose we have a constant glide ratio and by pulling risers we can control its yaw rate. Mathematically, this is expressed by the following simplified equations:

$$\dot{x} = V\cos\psi , \ \dot{y} = V\sin\psi , \ \dot{\psi} = v , \qquad (1)$$

where $v \in [-\Xi; \Xi]$ is the only control.

The Hamiltonian for the system (1) for a time-optimal control can now be written as:

$$H = p_\psi v + V(p_x, p_y)\begin{pmatrix} \cos\psi \\ \sin\psi \end{pmatrix} - 1, \qquad (2)$$

where equations for adjoint variables p_x, p_y and p_ψ are given by

$$\dot{p}_x = 0, \quad \dot{p}_y = 0,$$

$$\dot{p}_\psi = V(p_x, p_y)\begin{pmatrix} \sin\psi \\ -\cos\psi \end{pmatrix}. \qquad (3)$$

The optimal control for the time-minimum problem now is given by

$$v = \Xi\, sign(p_\psi). \qquad (4)$$

By differentiating the expression for $\dot{p}_\psi$ (3) and combining it with Hamiltonian (2) for both cases when $p_\psi > 0$ and $p_\psi < 0$ we can get a set of equations for p_ψ:

$$\ddot{p}_\psi + \Xi^2 p_\psi \mp \Xi = 0. \qquad (5)$$

This differential equation gives two sinusoids (shifted with respect to abscise axis by $\pm\Xi^{-1}$) as solutions for the general (non-singular) case

$$p_\psi = C_1 \sin(\Xi t + C_2) \pm \Xi^{-1}, \qquad (6)$$

where C_1 and C_2 are constants defined by the concrete boundary conditions. If $C_1 \neq \Xi^{-1}$ the parafoil model moves along a descending spiral. It takes $2\pi\Xi^{-1}$ seconds to make a full turn with a radius of $V\Xi^{-1}$. If $C_1 = \Xi^{-1}$ there exists a possibility of singular control. This is caused by the fact that there exists a point in time where both p_ψ and $\dot{p}_\psi$ are zero as can be seen from (6).

Consider singular control for this model. By definition it means that $p_\psi \equiv 0$. For the time-optimal problem from the Hamiltonian (2) and third equation in (3) (of course keeping in mind the first two) it follows that for a singular control case

$$p_x = V^{-1}\cos\psi, \; p_y = V^{-1}\sin\psi, \; \psi = const. \quad (7)$$

Expressions (7) imply that singular control corresponds to motion with a constant heading ($v \equiv 0$). It may not however be realized. Instead, the parafoil model may switch from right-handed spiral to a left-handed one or vice versa. Concrete boundary conditions define which case will be realized.

To summarize, as suggested by the Pontrjagin's principle of optimality [4] three-dimensional time-optimal trajectories would consist of helices (spiral descent) and straight descent segments. The basic difference between all possible trajectories is whether parafoil expends its potential energy at the beginning of descent or at the end. It may depend on the tactical conditions in the LZ, terrain, or some other factors. In a general case parafoil could spend its potential energy in the vicinity of some other waypoint differing from the start and final portions of the trajectory. In any case, since the control system cannot meet any time constraints due to unavailability of thrust on a parafoil system, the common feature of these reference trajectories

(RTs) is that they are defined in the inertial frame and are time independent.

Another critical issue is that in order to meet a soft-landing requirement the parafoil at the LZ must align itself into the wind.

III. REAL-TIME TRAJECTORY GENERATION

The optimal control analysis of the previous section motivated the basic RT structure as follows. This RT consists of three segments: initial straight-line glide (segment 1), spiral descent (segment 2) and final glide and flare (segment 3). Since it is required that the parafoil is aligned into the wind at LZ, the final glide segment ends at the desired impact point (DIP) and is directed into the wind. Furthermore, the final glide starts an offset distance d_{offset} away and a certain height above DIP. The height is determined by the flight path angle of the segment 3. Similarly, the first segment starts at the parafoil release point (RP) and ends at a point defined by the flight path angle of the first segment at the spiral descent segment. The first and last segments are fused together by the spiral descent segment. The radius of the spiral is adjusted to provide smooth transition between each segment. The rest of the section derives the mathematical representation of the complete RT.

Let γ_{RT_1} denote the desired flight path angle for the first straight-line segment of the trajectory, similarly let γ_{RT_2} denote the flight path angle for the spiral-descent segment and, finally, let γ_{RT_3} represent the flight path angle for the final straight-line segment. Furthermore, let ψ_f represent the wind direction at the LZ, $\mathbf{p}_0 = (x_0, y_0, z_0)^T$ is the RP, and $\mathbf{p}_f = (x_f, y_f, z_f)^T$ denotes the DIP. Define vector $\mathbf{i} = (\cos(\psi_f + \pi), \sin(\psi_f + \pi), 0)^T$ to be the unit vector that points into the wind at the LZ and vector $\mathbf{i}^* = (-\sin(\psi_f + \pi), \cos(\psi_f + \pi), 0)^T$ to be the unit vector orthogonal to $\mathbf{i}$. Then the initial point $\mathbf{p}_3 = (x_3, y_3, z_3)^T$ of the third segment is given by

$$\mathbf{p}_3 = -d_{offset}\mathbf{i} + (0, 0, z_f + d_{offset}\tan\gamma_{RT_3})^T. \qquad (8)$$

Now, let $\mathbf{p}_{RT}$ denote the position on the RT, s denote the path length traveled along the RT and V_{RT} - parafoil's velocity along this path. Then the expression for the third segment of the desired trajectory is

$$\mathbf{p}_{RT}(s) = \mathbf{p}_3 + \mathbf{T}_3 s, \; \dot{s} = V_{RT}, \qquad (9)$$

where

$$\mathbf{T}_3 = (-\cos\psi_f \cos\gamma_{RT_3}, -\sin\psi_f \cos\gamma_{RT_3}, -\sin\gamma_{RT_3})^T \quad (10)$$

is the unit vector that points along the line connecting $\mathbf{p}_3$ to $\mathbf{p}_f$. Note, that the length of the third segment $s_3 = \|\mathbf{p}_3 - \mathbf{p}_f\|$. Similarly, let s_1 denote the length of the

first segment and s_2 - of the second. Then, along the third segment ($s_1 + s_2 < s \le s_1 + s_2 + s_3$)

$$\mathbf{p}_{RT}(s) = \mathbf{p}_3 + \mathbf{T}_3 (s - s_1 + s_2). \qquad (11)$$

Next, consider Fig.1. Let r represent the radius of the spiral descent segment. Then the center of the spiral $\mathbf{p}_1 = (x_1, y_1, z_1)^T$ has the following expression

$$\mathbf{p}_1 = \mathbf{p}_3 + r\dot{\mathbf{i}}^*, \qquad (12)$$

which is used next to determine the expression for $\mathbf{p}_{RT}$ along segment 1. Let $d = \sqrt{(x_0 - x_1)^2 + (y_0 - y_1)^2}$, then

$\Delta\psi = \sin^{-1}\dfrac{r}{d}$, $\psi_1 = \tan^{-1}\dfrac{y_1 - y_0}{x_1 - x_0}$ and $\psi_2 = \psi_1 + \Delta\psi$.
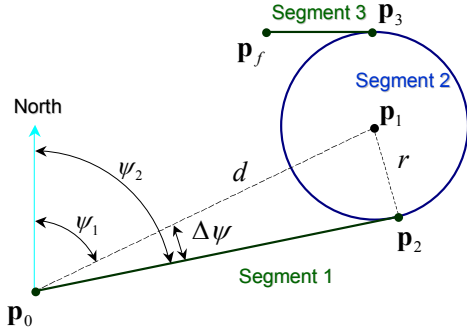

Fig.1 Top view of the parafoil RT

Analogous to (10) define

$$\mathbf{T}_1 = \left(\cos\psi_2 \cos\gamma_{RT_1}, \sin\psi_2 \cos\gamma_{RT_1}, -\sin\gamma_{RT_1}\right)^T. (13)$$

Then

$$\mathbf{p}_2 = \mathbf{p}_0 + \mathbf{T}_1 \frac{\sqrt{d^2 - r^2}}{\cos\gamma_{RT_1}}, \quad s_1 = \|\mathbf{p}_0 - \mathbf{p}_2\| \qquad (14)$$

and

$$\mathbf{p}_{RT}(s) = \mathbf{p}_0 + \mathbf{T}_1 s, \quad 0 \le s \le s_1. \qquad (15)$$

The turn rate $\dot{\psi}_{RT}$ along the spiral descent segment is given by

$$\dot{\psi}_{RT} = V_{RT} r^{-1} \cos\gamma_{RT_2}. \qquad (16)$$

Then, along the segment 2 ($s_1 < s \le s_1 + s_2$)

$$\mathbf{p}_{RT}(s) = \mathbf{p}_1 + \begin{pmatrix} r\sin\left(\rho_{RT}^*(s - s_1) + \Delta\right) \\ -r\cos\left(\rho_{RT}^*(s - s_1) + \Delta\right) \\ (s_1 - s)\sin\gamma_{RT_2} \end{pmatrix}, \qquad (17)$$

where $\rho_{RT}^* = \dot{\psi}_{RT} V_{RT}^{-1}$, $\Delta = \psi_f + \pi - \rho_{RT}^*(s_2 - s_1)$,

$s_2 = \dfrac{z_2 - z_3}{\sin\gamma_{RT_2}}$.

Without loss of generality, the z-component of the center of the spiral descent $\mathbf{p}_1$ was set to equal z_2 in the definition of $\mathbf{p}_{RT}(s)$ above.

Let

$$\mathbf{T}_2(s) = \frac{\dfrac{d\mathbf{p}_{RT}}{ds}}{\left\|\dfrac{d\mathbf{p}_{RT}}{ds}\right\|} = \begin{pmatrix} \cos\left(\rho_{RT}^*(s - s_1) + \Delta\right)\cos\gamma_{RT_2} \\ \sin\left(\rho_{RT}^*(s - s_1) + \Delta\right)\cos\gamma_{RT_2} \\ -\sin\gamma_{RT_2} \end{pmatrix}. (18)$$

Then, the choice of Δ guarantees that the horizontal projections of vectors defined by (18) and (10) are aligned, i.e.

$$\mathbf{T}_2^{hor}\big|_{s=s_2} = \mathbf{T}_3^{hor}\big|_{s=s_2} = \left(-\cos\psi_f, -\sin\psi_f\right)^T. \quad (19)$$

This fact implies that at $\mathbf{p}_3$ the horizontal projections of the commanded velocity vectors for segments 2 and 3 are equal and are independent of the choice of r.

Finally, the radius of the spiral descent r is selected to guarantee that at $\mathbf{p}_2$ segments 1 and 2 merge smoothly. This is done numerically by solving a single variable constrained optimization problem. Note that at $\mathbf{p}_2$

$$\mathbf{p}_{RT}\big|_{s=s_1} = \mathbf{p}_2 = \mathbf{p}_1 + \left(r\sin\Delta, -r\cos\Delta, 0\right)^T. \qquad (20)$$

Therefore, let

$$e(r) \doteq \left\|\mathbf{p}_2 - \mathbf{p}_1 + \left(r\sin\Delta, -r\cos\Delta, 0\right)^T\right\|, \qquad (21)$$

then the desired value of r is $r_{des} = \underset{r_{min} \le r \le r_{max}}{\arg\min} e(r)$. The values of r_{min} and r_{max} are selected to provide a unique solution that is consistent with physical limitations of the parafoil. Note, in steady state turn the bank angle of the parafoil is defined by the following expression:

$$\phi_{RT} = \tan^{-1}\frac{V_{RT}\dot{\psi}_{RT}}{g} = \tan^{-1}\left(\frac{V_{RT}^2 \cos\gamma_{RT_2}}{rg}\right), \quad (22)$$

where g is acceleration due to gravity. By construction the horizontal projections of $\mathbf{T}_1$ and $\mathbf{T}_2$ at $\mathbf{p}_2$ are aligned, i.e.

$\mathbf{T}_1^{hor}\big|_{s=s_1} = \mathbf{T}_2^{hor}\big|_{s=s_1}$.

IV. INTEGRATED GUIDANCE AND CONTROL ALGORITHM

The development of the integrated guidance and control algorithm presented in this section is based on the work reported in [2], where authors have proposed a new technique for tracking so-called trimming trajectories for unmanned air vehicle (UAV). As shown in this paper trimming trajectories consist of straight lines and helices. Therefore, this methodology is particularly suitable for the problem at hand.

The key ideas of the design methodology include the following five steps:
1) reparameterize trimming trajectory using the arclength s, thus eliminating time as an independent variable;
2) resolve the position and velocity errors in so-called Frenet frame;
3) form error dynamics for the system consisting of the trajectory and parafoil model, where the position and velocity error states are resolved in Frenet frame;
4) design a linear tracking controller for the linearization of the system along the trimming trajectory;

5) implement this controller with the true nonlinear plant using a nonlinear transformation provided in [2]. This implementation guarantees that the linearization along the trimming trajectory of the feedback system consisting of the nonlinear plant and nonlinear controller preserves the eigenvalues and transfer functions of the feedback interconnection of the linearized error dynamics and linear tracking controller [5].

A. Derivation of the errors in Frenet frame

As shown in Section III the desired RT is parameterized using the path/arclength parameter s.

Let $\mathbf{p} = (x, y, z)^T$ denote current position of the parafoil. The methodology presented above requires that position and velocity commands $\mathbf{p}_{RT}(s_*)$, $V_{RT}(s_*)$ used to compute position and velocity errors, $\mathbf{p}_{RT}(s_*) - \mathbf{p}$ and $V_{RT}(s_*) - V$ respectively, correspond to the point on the RT that is nearest to current position of the vehicle. This is done by first determining the value of the path/arclength parameter $s_* = \arg\min_s \|\mathbf{p}_{RT}(s) - \mathbf{p}\|^2$ and then using it to compute position and velocity commands. In [2] the problem of determining s_* is reduced to a constrained optimization problem. However, computing limitations of the onboard processor have imposed a need to develop analytical techniques for the computation of s_*, discussed next.

An exact analytical expression for s_* can be derived for straight-line segments 1 and 3. Recall (15) and (11). Then

$$s_* = \arg\min_s \left(\begin{matrix} \mathbb{R}, & 0 \le s \le s_1 \\ \mathbb{Q}, & s_1 + s_2 < s \le s_1 + s_2 + s_3 \end{matrix} \right), \quad (23)$$

where $\mathbb{R} = \|\mathbf{p}_0 + \mathbf{T}_1 s - \mathbf{p}\|$ and $\mathbb{Q} = \|\mathbf{p}_3 + \mathbf{T}_3 (s - s_1 - s_2) - \mathbf{p}\|$.

Simple algebra shows that for straight-line segments

$$s_* = \begin{cases} \mathbf{T}_1^T(\mathbf{p} - \mathbf{p}_0), 0 \le s \le s_1, \\ \mathbf{T}_3^T(\mathbf{p} - \mathbf{p}_3) + (s_1 + s_2), s_1 + s_2 < s \le s_1 + s_2 + s_3. \end{cases} \quad (24)$$

Now, recall that segment 2 represents a spiral. In this case, only an approximation of s_* can be found analytically. Its derivation is discussed next.

Let

$$C = \{(l, m, n) : (l - x_1)^2 + (m - y_1)^2 = r^2, z_1 \le n \le z_2\} \quad (25)$$

define a cylinder centered at $\mathbf{p}_1 = (x_1, y_1, z_1)^T$. Then the spiral descent trajectory

$$\mathbf{p}_{RT}(s) = \mathbf{p}_1 + \begin{pmatrix} r\sin\left(\rho_{RT}^*(s - s_1) + \Delta\right) \\ -r\cos\left(\rho_{RT}^*(s - s_1) + \Delta\right) \\ -(s - s_1)\sin\gamma_{RT_2} \end{pmatrix} \quad (26)$$

($s_1 < s \le s_1 + s_2$) is a subset of C. Furthermore, the projection of the vehicle's position $\mathbf{p}$ onto C is

$$\mathbf{p}_{proj} = \left((x_1, y_1) + r\frac{(x - x_1, y - y_1)}{\|x - x_1, y - y_1\|}, z \right)^T. \quad (27)$$

For any vector $\mathbf{p}_{cyl} = (x_{cyl}, y_{cyl}, z_{cyl})^T \in C$ define a function $\Pi : R^3 \to R^2$,

$$\Pi(\mathbf{p}_{cyl}) =: \begin{pmatrix} x_\Pi \\ z_\Pi \end{pmatrix} = \begin{pmatrix} r\tan^{-1}\left(\dfrac{x_1 - x_{cyl}}{y_1 - y_{cyl}} + \pi\right) \\ z_{cyl} \end{pmatrix}. \quad (28)$$

The function Π maps the cylinder C onto a rectangle of width $2\pi r$ and height $z_2 - z_1$. Moreover, the trajectory $\mathbf{p}_{RT}(s)$ defined for segment 2 is mapped into a function $\Pi(\mathbf{p}_{RT}(s))$ shown in Fig.2.
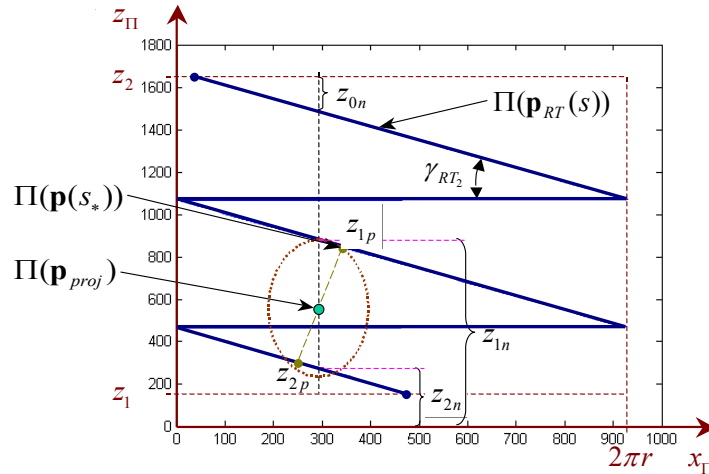

Fig.2 Graphical representation of the range of the function Π

Let d_* denote the distance from $\mathbf{p}$ to the nearest point $\mathbf{p}_{RT}(s_*)$ on the trajectory $\mathbf{p}_{RT}(s)$. Then $\mathbf{p}_{RT}(s_*)$ can be obtained by determining the intersection of the ball B_{d_*} of radius d_* centered at $\mathbf{p}$. The mapping $\Pi(B_{d_*} \cap C)$ is an

ellipse centered at $\Pi(\mathbf{p}_{proj})$ with semi-major and semi-minor radii given by $r_z = d_x \sqrt{3}$ and $r_x = r \cos^{-1} \dfrac{r^2 + (r+d_x)^2 - 4d_x^2}{2r(r+d_x)}$, respectively. In the previous expressions $d_x = (x - x_{proj})^2 + (y - y_{proj})^2$. Intersection of this ellipsoid with $\Pi(\mathbf{p}(s))$ represents the mapping $\Pi(\mathbf{p}(s_*))$ of $\mathbf{p}(s_*)$. Analytical approximation of $\Pi(\mathbf{p}(s_*))$ is obtained next and then used to compute s_*.

Consider Fig.2. Note for the case illustrated in this figure, the z_Π coordinate of $\Pi(\mathbf{p}(s_*))$ is bounded above by z_{1n} and below by z_{1p}. Using the basic geometry shown in Fig.2, expressions for z_{1n} and z_{1p} are:

$$
\begin{aligned}
z_{1n} &= z_{proj} + \left| \mathrm{mod}(z_{0n} - z_{proj}, 2\pi r \tan \gamma_{RT_2}) \right|, \\
z_{1p} &= z_{proj} + \left| z_{1n} - z_{proj} \right| \cos^2 \gamma_{RT_2},
\end{aligned}
\tag{29}
$$

where

$$
\begin{aligned}
z_{0n} &= z_1 - s_{*n} \sin \gamma_{RT_2}, \\
s_{*n} &= \rho_{RT}^* \left(\frac{x_{proj}}{r} - \mathrm{mod}(\Delta, 2\pi) \right).
\end{aligned}
\tag{30}
$$

Similarly,

$$
\begin{aligned}
z_{2n} &= z_{1n} - 2\pi r \tan \gamma_{RT_2}, \\
z_{2p} &= z_{proj} - \left| z_{2n} - z_{proj} \right| \cos^2 \gamma_{RT_2}.
\end{aligned}
\tag{31}
$$

The variables z_{2p} and z_{1p} represent the z-coordinates of the projections of $\Pi(\mathbf{p}_{proj})$ onto the two nearest legs of $\Pi(\mathbf{p}(s))$. These variables can now be used to find the approximation of z_Π, z_{app}:

$$
z_{app} = \begin{cases} z_{1p}, & \text{if } \left| z_{1p} - z_{proj} \right| < \left| z_{2p} - z_{proj} \right|, \\ z_{app} = z_{2p}, & \text{otherwise.} \end{cases}
\tag{32}
$$

Note that logic (32) guarantees that in the case when two legs of $\mathbf{p}(s)$ are equidistant from $\mathbf{p}$, the point closer to the ground is selected. Furthermore, since Π maps z-axis of R^3 onto itself z_{app} can be used to compute s_*

$$
s_* = \frac{z_1 - z_{app}}{\sin \gamma_{RT_2}},
\tag{33}
$$

which follows from the definition of $\mathbf{p}(s)$ for the spiral descent segment. This value of s_* can now be used to compute the unit basis vectors $\mathbf{T}_2$, $\mathbf{N}_2$, and $\mathbf{B}_2$ of the Frenet frame $\{F\}$ for segment 2 at $s = s_*$

$$
\mathbf{T}_2 = \frac{\dfrac{d\mathbf{p}_c}{ds}}{\left\| \dfrac{d\mathbf{p}_c}{ds} \right\|}, \quad \mathbf{N}_2 = \frac{\dfrac{d\mathbf{T}_2}{ds}}{\left\| \dfrac{d\mathbf{T}_2}{ds} \right\|}, \quad \mathbf{B}_2 = \frac{\mathbf{T}_2 \times \mathbf{N}_2}{\left\| \mathbf{T}_2 \times \mathbf{N}_2 \right\|}
\tag{34}
$$

or in the final form

$$
\mathbf{T}_2(s_*) == \begin{pmatrix} \cos\left(\rho_{RT}^*(s_* - s_1) + \Delta \right) \cos \gamma_{RT_2} \\ \sin\left(\rho_{RT}^*(s_* - s_1) + \Delta \right) \cos \gamma_{RT_2} \\ -\sin \gamma_{RT_2} \end{pmatrix},
$$

$$
\mathbf{N}_2(s_*) == \begin{pmatrix} -\sin\left(\rho_{RT}^*(s_* - s_{\lim_1}) + \Delta \right) \\ \cos\left(\rho_{RT}^*(s_* - s_1) + \Delta \right) \\ 0 \end{pmatrix},
\tag{35}
$$

$$
\mathbf{B}_2(s_*) = \frac{\mathbf{T}_2(s_*) \times \mathbf{N}_2(s_*)}{\left\| \mathbf{T}_2(s_*) \times \mathbf{N}_2(s_*) \right\|}.
$$

For segments 1 and 3 the basis vectors are constant. For example, for segment 1 we obtain

$$
\mathbf{T}_1 = \begin{pmatrix} \cos \psi_2 \cos \gamma_{RT_1} \\ \sin \psi_2 \cos \gamma_{RT_1} \\ -\sin \gamma_{RT_1} \end{pmatrix}, \quad \mathbf{N}_1 = \begin{pmatrix} -\sin \psi_2 \\ \cos \psi_2 \\ 0 \end{pmatrix},
\tag{36}
$$

and for segment 3

$$
\mathbf{T}_3 = \begin{pmatrix} -\cos \psi_f \cos \gamma_{RT_3} \\ -\sin \psi_f \cos \gamma_{RT_3} \\ -\sin \gamma_{RT_3} \end{pmatrix}, \quad \mathbf{N}_3 = \begin{pmatrix} \sin \psi_f \\ -\cos \psi_f \\ 0 \end{pmatrix}.
\tag{37}
$$

The basis vectors $\mathbf{B}_1$ and $\mathbf{B}_3$ are computed exactly as $\mathbf{B}_2$. Now the rotation matrix ${}_{LTP}^{F}R_i$ from LTP to Frenet frame for the i-th segment is given by ${}_{LTP}^{F}R_i = (\mathbf{T}_i, \mathbf{N}_i, \mathbf{B}_i)^T$ and the corresponding position and velocity errors are

$$
\begin{aligned}
\mathbf{p}_e &= {}_{LTP}^{F}R_i (\mathbf{p}_{RT}(s_*) - \mathbf{p}) =: (0, y_e, z_e)^T, \\
\dot{\mathbf{p}}_e &= {}_{LTP}^{F}R_i (\dot{\mathbf{p}}_{RT}(s_*) - \mathbf{V}) + {}_{LTP}^{F}\dot{R}_i (\mathbf{p}_{RT}(s_*) - \mathbf{p}).
\end{aligned}
\tag{38}
$$

(Notice that by construction the x-component of the position error vector $\mathbf{p}_e$ is zero. These error vectors were used to design a tracking control system discussed in the next section.)

B. Control System Design

The trajectory tracking controller design methodology proposed in [2] is now applied to the design of a tracking controller for the trajectory generated using the algorithm developed in Section III. The controller can only use GPS position and velocity for feedback. This constraint is motivated by the requirement to keep the cost of the onboard avionics low, therefore, only GPS is available for control.

During segments 1 and 2 the control system uses differential flaps to drive the lateral components of the position and velocity error vectors to zero. On the other hand, the last segment is tracked using both symmetric and differential flaps, denoted here by δ_S and δ_D, respectively. The structure of tracking controller for the lateral channel shown is Fig.3.

The gains K_y and $K_{\dot{y}}$ shown in Fig.3 were selected to provide stability and performance for the lateral channel of the feedback system. The variables z^{-1} and T denote backward shift and sampling period. The onboard GPS

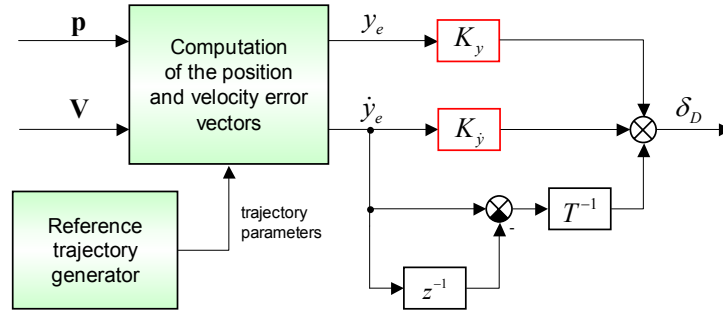receiver, whose update rate is $2Hz$, dictated the sampling period for this problem.

Fig.3 Lateral channel tracking controller structure

The vertical channel controller uses symmetric flaps δ_S to drive the vertical channel error to 0 and was only used to track the final segment of the trajectory. This decision was motivated by the fact that symmetric flaps have negligible control authority in spiral descent. Furthermore, deflecting symmetric flaps tends to increase the descent rate of the parafoil while reducing the flap deflection budget available for differential flaps command and, therefore, symmetric flaps were not used during segment 1 as well.

V. SIMULATION RESULTS

The trajectory tracking control system discussed in the previous section has been tested in simulation. Fig.4 shows an example of such simulation based on the 6DoF model discussed above. Each of 40 simulation runs included the real wind profile obtained at YPG.
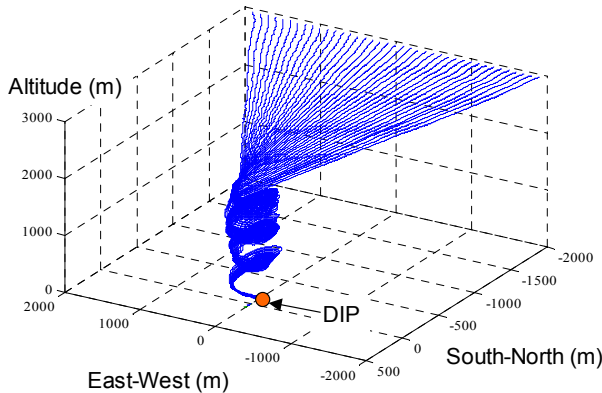

Fig.4 Simulation results of the trajectory tracking control system

The GPS position and velocity errors were modeled as white noise processes with zero mean and standard deviations (STD) shown in Tab.1. Finally, landing performance statistics shown in Tab.2 indicate that system's performance exceeded the required circular error probable (CEP) of $100m$.

TABLE 1 GPS errors (STD)

	x-direction	y-direction	z-direction
Position (m)	5	5	10
Velocity (m/s)	0.3	0.3	0.5

TABLE 2 Touchdown errors

CEP (m)	Mean value (m)	STD (m)
70.7	67.5	20.5

VI. CONCLUSIONS

The optimal control strategy for the Pegasus parafoil payload delivery system was synthesized based on Pontrjagin's maximum principle. This motivated the structure of the real-time reference trajectory generator. Together with the robust path following algorithm it enabled a successful development and simulation testing of the complete guidance and control algorithm.

VII. REFERENCES

[1] I.Kaminer and O.Yakimenko, "Development of Control Algorithm for the Autonomous Gliding Delivery System", *in 17th AIAA Aerodynamic Decelerator Systems Technology Conference*, Monterey, CA, May 19-22, 2003.

[2] I.Kaminer, A.Pascoal, E.Hallberg and C.Silvestre, "Trajectory Tracking for Autonomous Vehicles: An Integrated Approach to Guidance and Control", *Journal of Guidance, Control, and Dynamics,* vol.21 (1), 1998, pp.29-38.

[3] P.Mortaloni, O.Yakimenko, V.Dobrokhodov, and R.Howard, "On the Development of Six-Degree-of-Freedom Model of Low-Aspect-Ratio Parafoil Delivery System", *in 17th AIAA Aerodynamic Decelerator Systems Technology Conference*, Monterey, CA, May 19-22, 2003.

[4] L.Pontrjagin, V.Boltjanskiy, R.Gamkrelidze and E.Mishenko, *Mathematical Theory of Optimal Processes*, Nayka, Moscow, 1969 (in Russian).

[5] D.Costello, I.Kaminer, K.Carder, and R.Howard, "The Use of Unmanned Vehicle Systems for Coastal Ocean Surveys: Scenarios for Joint Underwater and Air Vehicle Missions", *in Workshop on Intelligent Control of Autonomous Vehicles*, Lisbon, Portugal, 1995, pp.61-72.